

Simulation of point defects in high-density luminescent crystals: Oxygen in barium fluoride

J. M. Vail, E. Emberly, and T. Lu

Department of Physics, University of Manitoba, Winnipeg, Canada, MB R3T 2N2

M. Gu

Department of Physics, Tongji University, Shanghai 200092, People's Republic of China

R. Pandey

Department of Physics, Michigan Technological University, Houghton, Michigan 49931

(Received 18 June 1997; revised manuscript received 25 August 1997)

Barium fluoride is an example of a high-density scintillator for detecting high-energy radiation. In use, its luminescent transmission is seriously degraded by radiation damage. This effect is associated with oxygen, among other impurities. At one time it was suspected that oxygen O^- , having been dissociated from a defect complex by radiation damage, absorbed some of the luminescent energy of the crystal. This explanation has now been abandoned, and the present work shows quantitatively that it is not correct. Specifically, a detailed study of the optical absorption of O^- shows that its excitation energy, split by spin polarization, is $\sim 50\%$ higher than the luminescent frequencies of the crystal. Instead, color centers, such as F centers, have come to be suspected. One origin of the color center is shown here to be the dissociation of a defect complex made up of an O^{2-} ion bound to a fluoride vacancy, accompanied by electron transfer from oxygen to vacancy, forming an F center. The study of the optical excitation of O^- is used to assess the qualitative and quantitative importance of the main elements of the physical model and computational method in such a simulation. These elements include the ion-size effect of Ba^{2+} ions, spin-polarization effects in ground and excited states, electric quadrupole moment consistency between the O^- ion and the embedding BaF_2 crystal, basis set augmentation and optimization in the treatment of a quantum molecular cluster that includes the impurity for both ground and excited states, correlation correction, and projection of excited states onto spin eigenstates. [S0163-1829(98)04202-7]

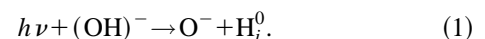
I. INTRODUCTION

Barium fluoride, BaF_2 , is an important representative of a class of high-density luminescent materials used for γ ray and elementary particle detection.¹ In practical terms, another crystal, $PbWO_4$, is of more immediate interest, so our Manitoba-Shanghai-Michigan Tech collaboration includes a detailed study of its defect properties.² (The densities of BaF_2 and $PbWO_4$ are 4.88 and 8.28 g/cm³, respectively.) The present study of BaF_2 is intended to be primarily methodological, providing the experience and technical background upon which to pursue detailed results for $PbWO_4$, and ultimately for other similar ionic crystals. Our choice of defect and processes reflects this objective, and is not focused on the principal feature of technical interest for BaF_2 . In particular, we do not analyze the optical absorption of the F center in BaF_2 . Furthermore, we do not examine the excitation from the valence band of the crystal to the unoccupied p_z level of the O^- impurity, for which we show that there is reason to consider it.

Barium fluoride has fast luminescent components at 195 and 220 nm.³ A cross-luminescence process has been identified, involving a transition from the first valence band (F^- - $2p$ -like) into a hole, arising from irradiation, in the Ba^{2+} core band.⁴ The luminescence is degraded by color centers that arise in irradiation damage.⁵ These color centers reduce the crystal's transmissivity by absorbing the luminescent emission. The damage is not intrinsic; that is, it does not

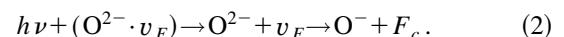
affect the basic luminescent mechanism, but the luminescence recovers only very slowly at room temperature.^{3,5} A variety of damage processes that produce color centers are of interest, involving rare-earth and oxygen impurities.⁶ In the present work we concentrate on oxygen.

There is a number of damage processes in which the production of color centers is associated with the production of monovalent oxygen, O^- . One class of such processes involves electron loss by impurity metal ions.^{6,7} Another process involves dissociation of an hydroxyl molecular ion $(OH)^-:$ ⁶



In Eq. (1), H_i^0 is a neutral interstitial hydrogen atom. We shall not analyze these processes in the present work.

A further process is dissociation of oxygen-vacancy complexes:^{8,9}



In Eq. (2), v_F is a fluoride-site vacancy with net positive charge relative to the host crystal. It is bound to an O^{2-} ion, forming an electric dipole defect complex in the crystal. In the radiation damage process, energy $h\nu$ is absorbed by the defect complex, the vacancy separates from the oxygen ion by step diffusion, and energy is minimized by electron transfer from oxygen to vacancy, resulting in an F center, denoted F_c . In the present work, rudimentary calculations will esti-

mate the activation energy for $(\text{O}^{2-} \cdot v_{\text{F}})$ dissociation, and will compare the energies of separated O^{2-} and v_{F} defects on one hand, and of separated O^- and F_c defects on the other.

The electronic structure of pure BaF_2 has been analyzed theoretically by Ermakov and co-workers⁴ and by Andriessen and co-workers.¹⁰ The former used the continued fraction method applied to a Green's function derived for a cluster of 21 atoms. The latter studied clusters embedded in a point-ion crystal at the Hartree-Fock self-consistent-field level of approximation, based largely on gaussian basis sets from Huzinaga¹¹ in a standard linear combination of atomic orbitals-molecular orbitals (LCAO-MO) analysis. Cross luminescence was discussed for both pure and Ce^{3+} -doped BaF_2 . The theoretical approach of the present work is similar to that of Andriessen and co-workers in using a cluster of ions embedded in a classical crystal, with gaussian basis sets for the Hartree-Fock self-consistent-field (SCF) analysis. It differs, however, by including self-consistent relaxation and polarization of the classical embedding crystal in the case of defects, by using systematically optimized basis functions for each state of the defect, and by including correlation corrections explicitly.

The present work arises from an interest in the radiation damage process represented in Eq. (2). Originally, optical excitation of either of the products, O^- or F_c , were considered as candidates for the absorption of the BaF_2 luminescence. Experimental analysis has now eliminated O^- as a candidate. Here we present a detailed analysis of O^- absorption in BaF_2 . The results bear out the experimental conclusion, showing that absorption by O^- occurs at a higher frequency than BaF_2 luminescence. The absorption splitting by the spin polarization of O^- is an interesting feature of this system, and is studied in detail.

In Sec. II we describe our physical model, our theoretical method, and details of our computational approach. In Sec. III, quantitative results for the ground and excited states of substitutional O^- in BaF_2 are given, and the optical excitation process is described. A brief critique of the method is given at this point. In Sec. IV, less polished calculations than those of Sec. III are used to analyze the energetics of Eq. (2), the radiation damage process in which free O^- ions and F centers are produced. The results show that electron transfer from O^{2-} to v_{F} is energetically favored upon dissociation of the $(\text{O}^{2-} \cdot v_{\text{F}})$ defect complex. In Sec. V our results are summarized.

II. MODEL AND METHOD

BaF_2 has the fluorite structure, and we consider O^- substitutional at a fluoride site. It then has four nearest-neighbor F^- ions: see Fig. 1. We anticipate that first- and/or second-neighbor ions may be involved in the optical excitation process. We therefore base our quantum-mechanical analysis of the system on the cluster of eleven ions shown in Fig. 1. The rest of the crystal will be represented by the shell model, in which each ion is represented by two point charges, harmonically coupled, one of which is called the core, the other the shell. Interionic interactions consist of Coulomb and short-range forces, the latter, of the Buckingham type $V(r)$, acting between shells, being given by

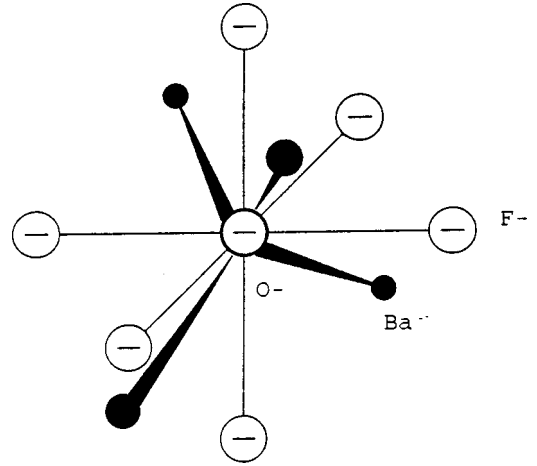


FIG. 1. Oxygen O^- substitutional impurity in BaF_2 crystal, showing its four nearest Ba^{2+} and six second F^- neighbors.

$$V(r) = \{B \exp(-r/\rho) - Cr^{-6}\}. \quad (3)$$

The parameters (B, ρ, C) in Eq. (3) are determined, for each pair of ionic species, along with shell charge Y and shell-core coupling constant K , for each ionic species, by fitting to bulk properties of the crystal. Values of these parameters, from Catlow and co-workers,¹² are given in Table I. For the F^- - F^- interaction, (B, ρ, C) were fitted to the form given in Ref. 12.

The quantum cluster surrounding the O^- impurity, and the shell-model crystal that embeds it, are used together in calculations that we describe as the ICECAP method. The ICECAP program^{13,14} determines the ground state of a point defect in an ionic crystal by relaxing atomic positions in the cluster, and ionic cores and shells in the embedding crystal, to equilibrium in the sense that the shell-model ions see the electric monopole moments of ions in the cluster, and the electrons in the cluster see the shell-model ions. In the case of O^- , we shall find that it has a quadrupole moment. In that case, the shell-model ions are made to see a symmetrical linear array of three charges to represent both monopole and prolate quadrupole moments of O^- , the latter being progressively adjusted to achieve total energy minimization. Specifically, a central point charge $(Q - 2q)$, where $Q = -1$ is the monopole moment of O^- , and two symmetrically placed charges $+q$, induce a polarization field in the embedding crystal. This produces a particular quantum cluster solution. q is then varied, with a new cluster solution for each value, until total energy of the quantum cluster and the embedding crystal is a minimum.

Now consider the quantum cluster, Fig. 1. O^- has 9 electrons, F^- has 10, and Ba^{2+} has 54, for a total of 285. This is

TABLE I. Shell-model parameters for BaF_2 , from Ref. 12.

	B (eV)	ρ (Å)	C (eV Å ⁶)
Ba-F	5193.3	0.2795	
F-F	1482.61	0.29329	53.17
	Y ($ e $)	K (eV Å ⁻²)	
Ba^{2+}	-16.99	1709.1	
F^-	-1.59	43.5	

too many for the kind of detailed optical excitation analysis that we have in mind. Our approach will be based on the unrestricted Hartree-Fock (UHF) SCF method. This will be followed by second-order Rayleigh-Schrödinger many-body perturbation theory (MBPT) correlation correction. The precise method is given by Thouless,¹⁵ and details of its application to the Hartree-Fock method are given by Vail.¹⁶ We can easily deal with all the electrons of O^- and of six F^- ions. We consider two levels of compromise in the treatment of the four Ba^{2+} ions, namely as point charges and as full-core pseudopotentials. For the latter we adopt Kunz-Klein localizing potentials (KKLP).^{17,14} Preliminary estimates were made of the excitation energies, giving 7.26 and 6.86 eV in the case of point charge Ba^{2+} ions, and 12.44 and 10.76 eV with KKLP. These calculations were performed at the Hartree-Fock level, with quadrupole consistency, spin projection, optimization of the $O^- 3s$ orbital, and omitting $F^- 3p$ and $3d$, and $O^- 3d$ orbitals. Not only is there a large difference in these excitation energies between the two treatments of Ba^{2+} , but the nature of the excitation processes are fundamentally different. Specifically, with the point charge Ba^{2+} , the excitations are both from $F^- 2p$ to $O^- 3s$ orbitals, while for KKLP Ba^{2+} they are both from $O^- 2p$ to $Ba^{2+} 6s$ orbitals. Since the KKLP gives a more accurate physical picture of the Ba^{2+} core, we use it in all calculations reported below.

In order to perform the analysis with point-charge Ba^{2+} ions, it was necessary to have a short-range Ba^{2+} - O^- Buckingham potential. We therefore considered the linear quantum cluster $F^- Ba^{2+} O^-$, in all-electron treatment, embedded in a relaxed shell-model BaF_2 crystal, using the ICECAP method. By varying the Ba^{2+} ion's position, we fit the energy variation of the embedded cluster to that of its shell-model representation. Keeping the F^- - Ba^{2+} interaction from BaF_2 , the parameters of the O^- - Ba^{2+} Buckingham potential were determined from the fitting to be $B = 7479.39$ eV, $\rho = 0.3192$ Å, and $C = 997.456$ eV Å⁶.

We now give necessary details of the UHF-SCF method.^{18,14} It is governed by the Fock equation for a cluster containing N electrons:

$$F|j\rangle = \varepsilon_j|j\rangle, \quad j = 1, 2, \dots, N, \quad (4)$$

where, in Bohr-Hartree atomic units:

$$F(\mathbf{r}) = \left\{ -\frac{1}{2} \nabla^2 + \sum_{j=1}^N \langle j | (|\mathbf{r} - \mathbf{r}'|^{-1}) (1 - P) | j \rangle + V(\mathbf{r}) \right\}. \quad (5)$$

The SCF term involves $(1 - P)$ where $P \equiv P(\mathbf{r}, \mathbf{r}')$ is the pairwise interchange operator. In the present case, the single-electron potential $V(\mathbf{r})$ arises from three sources: (1) bare nuclei of O^- and F^- ions in the cluster; (2) KKLP cores of Ba^{2+} ions in the cluster; (3) point-charge shell-model cores and shells of the embedding crystal.

The Fock equation (4) is solved variationally. The eigenstates $|j\rangle$ are taken to be MO, represented in position and spin space by

$$\phi_j(\mathbf{r}, s) = \psi_j(\mathbf{r}) \eta_j(s), \quad (6)$$

where $\eta_j(s)$ is a spin eigenstate. The position space part, $\psi_j(\mathbf{r})$, is expanded as a LCAO, $\{\chi_k(\mathbf{r})\}$:

$$\psi_j(\mathbf{r}) = \sum_k a_j(k) \chi_k(\mathbf{r}). \quad (7)$$

The AO, $\chi_k(\mathbf{r})$, are each localized about a single site, \mathbf{R}_k in the cluster. In the present work, these are all ionic sites. Specifically,

$$\chi_k(\mathbf{r}) = \sum_i d_i(k) \exp(-\alpha_i(k)|\mathbf{r} - \mathbf{R}_k|^2) Y_{l(k)}^{m(k)}(\Omega). \quad (8)$$

In Eq. (8) we see that the angular dependence of each AO is given by a spherical harmonic $Y_{l(k)}^{m(k)}(\Omega)$, where Ω are spherical polar angular variables, and that the radial dependence relative to site \mathbf{R}_k is a linear combination of gaussians, with exponential coefficients $\alpha_i(k)$. The linear coefficients $d_i(k)$ are called contraction coefficients. For given k , the sets of coefficients $\{d_i(k), \alpha_i(k)\}$ are fixed during the solution of the Fock equation. The AO basis set $\{\chi_k(\mathbf{r})\}$ are taken to be the nonorthogonal basis for a matrix representation of the Fock equation (4). To have N eigenstates, it requires that the dimensionality of $\{\chi_k\}$ be $\geq N$. In the present work it is $> N$. For the ground state of the system, the N eigenstates with the lowest values of ε_j are referred to as occupied, and are used in the SCF, and in determining the N -electron total energy and Slater determinant wave function. The remaining Fock eigenstates, called virtual states, are used to construct excited states of the N -electron system, both for the description of optically excited states, and for evaluating the MBPT correlation correction.

Compilations exist for exponential $\{\alpha_i(k)\}$ and contraction $\{d_i(k)\}$ coefficients that have been optimized in calculations for free atoms and ions: see, for example, Huzinaga (1985).¹¹ We generally use these as a starting point for our calculations, but we then proceed to reoptimize them in their crystalline environment as represented in the ICECAP method. Here, reoptimization means minimization of the total energy of the crystal, consisting of quantum cluster and embedding shell-model regions, neglecting correlation and spin projection. These minimizations are very time consuming, since the manifold of variables $\{\alpha_i(k), d_i(k)\}$ is multidimensional and the dependence on $\{\alpha_i(k)\}$ is nonlinear. For each choice of values of $\{\alpha_i(k), d_i(k)\}$, the full SCF solution of the Fock equation must be carried out. In general, the reoptimization process consists of varying a given parameter until the nearest energy minimum is located, repeating with the next variable, through the full range of variables, and then iterating to convergence to an accuracy of ~ 0.01 eV in total energy. We shall see that this process is essential to get physically accurate results.

There is an important constraint that we have applied to these reoptimization processes. It has to do with the boundary conditions for the quantum cluster. For a free molecule, one can vary the localization parameters (exponential coefficients) $\alpha_i(k)$ freely, using the minimum-energy principle to optimize them. For a molecular cluster embedded in a crystal, the nature of the boundary condition is complicated, having to do, first, with the localization of N orbitals from the crystal into the small cluster region, and second, with overlap

effects between ions in the cluster and embedding regions. In the present work, the classical shell-model representation of the embedding region does not provide any of the Pauli repulsion that quantum-mechanical electrons in the cluster would experience from electrons in the embedding region. Under the variational principle, the cluster electrons tend to spread out into the embedding region in an unphysical way. This effect not only leads to incorrect total-energy values, but to unphysical electronic configurations, and incorrect pictures of electronic defect processes. We believe that neglect of this effect may already have produced some incorrect interpretations of simulation studies. For a free molecule, one can decontract an atomic orbital, Eqs. (7) and (8), treating the products $a_j(k)d_i(k)$ as independent linear variables. For an embedded cluster, this procedure results in the linear coefficients of the smallest $\alpha_i(k)$, the longest-range gaussians, becoming too dominant in the AO. We combat this tendency by keeping the AO contracted [the $d_i(k)$'s fixed], during the variation of an $\alpha_i(k)$. In most cases we find that we can successively vary one $\alpha_i(k)$, then the corresponding (largest) $d_i(k)$, proceeding to the next value of i , and so on, iterating to convergence without producing runaway delocalization. When this is not achievable, we eliminate the dominant $d_i(k)$ from the variational procedure, not allowing it to grow relative to the others. The exception to these methods is when we are establishing a reoptimized basis set for F^- . In that case, we consider the perfect crystal, and the F^- ion at the center of an embedded cluster $(F^-)_7(Ba^{2+})_4$ is decontracted and recontracted, an orbital at a time, with the outer six F^- ions frozen in free-ion contractions. The new set of contractions from the central ion are then transferred to the outer six, and the process is iterated to convergence. In this case, the central ion is always subject to Pauli repulsion from its six neighbors, so it does not need to be artificially constrained. While the artificial constraint of outer-ion orbitals is clearly an *ad hoc* procedure, it is physically reasonable and demonstrably necessary. Ultimately, within this methodology, one will include the electronic structure of the embedding crystal in some realistic but manageable way. Much formal work has been done on this problem, and a significant body of explicit simulation has also been done with such an approach, including the optical properties of impurities. A recent review of one such body of work is the paper by Seijo and Barandiaran.¹⁹ Since our excited states involve both nearest-neighbor Ba^{2+} ions and second-neighbor F^- ions, the set of their nearest neighbors in the embedding crystal, numbering thirty-eight, would need to be included, at a minimum. Presently, even to describe these ions by Kunz-Klein localizing potentials would be prohibitive in terms of computer time, with the present method.

We now consider the AO basis set specifically for the present problem. For the ground state, free-atom considerations suggest that the following atomiclike orbitals would be required. For F^- , $1s^2 2s^2 2p^6$, and for oxygen, taking account of the fact that spin polarization arising from the odd number of electrons renders one coordinate direction, say z , distinct from the other x, y directions, we have $1s^2 2s^2 2p_{x,y}^4 2p_z^1$. At this point we can see why O^- has a quadrupole moment: it has a $2p_z$ -like hole in an otherwise filled-shell configuration. *A priori*, the nature of the excitation process is unknown. It may come from the O^- ion, or its

F^- neighbors, or from both. (We cannot include Ba^{2+} as a source of excitation because it is not represented by quantum-mechanical electrons, but by a pseudopotential core.) The excitation may be to O^- , Ba^{2+} , or F^- orbitals, or a combination of them, that are unoccupied in the ground state. In fact, we shall find that the highest-energy [ϵ_j , Eq. (4)] occupied Fock eigenstate in the ground state is predominantly $O^- 2p_{x,y}$ -like, in both spin-up and spin-down manifolds. That being so, the electric dipole excitation may involve the following: $F^- 3s, 3p$, and $3d$ levels, $O^- 3s$ and $3d$ levels, and $Ba^{2+} 6s$ and $5d$ levels. Although higher levels may also participate, we cannot include them because of computational practicalities. For the same reason, we include $Ba^{2+} 6s$ and $5d$ orbitals only in separate calculations, not together.

For mathematical consistency, the basis sets in both ground and all excited states need to be comparable. All of the above orbital types are included (except for $Ba^{2+} 6s$ or $5d$) in all calculations that are used to estimate transition energies. This means that, with respect to angular variables Ω , Eq. (8), the same functional manifold is used in all such calculations. Because the contraction and exponential coefficients $\{d_i(k), \alpha_i(k)\}$ are separately optimized in each many-body state, ground and excited, different functional manifolds for the radial variable are used for different states. However, the number of primitive AO, i.e., the number of distinct $\alpha_i(k)$, is the same throughout. The variational procedure then amounts to optimizing the radial manifold for each state separately, where all such manifolds have the same dimensionality, and also optimizing within each such manifold. Optimizing the radial manifolds separately for each state has the effect of reducing the calculated excitation energies (at Hartree-Fock level, without spin projection or correlation correction) by 25–30% (~ 3.4 – 3.9 eV). It is therefore certainly of quantitative significance for the simulation. One might feel that using different manifolds variationally for different states is mathematically inconsistent. However, that it is nevertheless appropriate may be seen from the following argument. If one were to use the union of manifolds obtained here from *all* states, the effect say, of additional basis functions from an excited state on the ground state would be small due to the fact that it comes from a function whose angular manifold contributes only weakly to the ground state.

We next consider some specifics about the excited states. The ICECAP program allows us to analyze an excited state in the presence of the equilibrium ionic configuration of the ground state: the product of a Franck-Condon transition. The Hartree-Fock part of the program includes the unrestricted form, in which spin-up and spin-down manifolds are solved separately using, of course, a common SCF. This leads to spin polarization in the case where the numbers of spin-up and spin-down electrons are different, as here. This means that spin-up and spin-down Fock eigenstates do not occur in identical pairs.

Our quantum cluster contains 69 electrons, which in the ground state are 35 spin up and 34 spin down. We represent this as follows:

ground: up (11111000)
down (11110000).

Such a picture omits the first thirty occupied Fock eigenstates, of both up and down spins, showing an excess of one spin up, and the first few of an infinite number of virtual, unoccupied states, the zeros. There are four excited states that can be considered, denoted (a), (b), (c), and (d) as follows:

excited:	(a)	up	(1 1 1 1 1 1 0 0)
		down	(1 1 1 0 0 0 0 0),
	(b)	up	(1 1 1 1 0 1 0 0)
		down	(1 1 1 1 0 0 0 0),
	(c)	up	(1 1 1 1 1 0 0 0)
		down	(1 1 1 0 1 0 0 0),
	(d)	up	(1 1 1 1 0 0 0 0)
		down	(1 1 1 1 1 0 0 0).

Cases (a) and (d) represent forbidden transitions, in dipole approximation. Cases (a), (b), (c), and (d) are in order of increasing energy. Cases (b) and (c) are allowed, representing excitations in the spin-up and spin-down manifolds respectively, relative to the ground state as represented above. Because the total spin is not zero, these excitations are not equal: the optical absorption line is split due to the quadrupole moment of O^- in the ground state.

The SCF Hartree-Fock solutions for cases (a) and (d) have total spins of 1.5 and 0.5, respectively, in units of \hbar . Similarly the ground state is given as a spin- $\frac{1}{2}$ state to reasonable accuracy ($<2\%$). However, at the same level, the calculated total spins of cases (b) and (c) are not 0.5; rather they are given by 0.918 and 0.853, respectively. The reason is that the corresponding solutions are linear combinations of cases (b) and (a), and of (c) and (a), respectively. Our procedure has been to evaluate the correlation corrections for the mixed-spin states, and then to project out case (a) from the resultant many-electron eigenstates and eigenvalues. If E'_b and s' are the mixed-spin state energies and spin, E_b is the pure spin- $\frac{1}{2}$ excited state energy, and E_a the pure spin- $\frac{3}{2}$ forbidden excited states energy, then one finds

$$E_b = \frac{\left\{ E'_b - \left[\frac{1}{3} s'(s'+1) - \frac{1}{4} \right] E_a \right\}}{\left[\frac{5}{4} - \frac{1}{3} s'(s'+1) \right]}. \quad (9)$$

The same equation, with c replacing b , applies for case (c). We shall see that projection onto spin eigenstates produces significant corrections to the excitation energies and their splitting.

III. RESULTS: OPTICAL EXCITATION

In Sec. II we explained that substitutional O^- impurity in BaF_2 has a prolate electric quadrupole moment due to a $2p$ -like electron hole. The explicit value of the point-charge simulator q , displaced along the z axis by ± 0.2 times the interionic spacing of the anion sublattice, was found to be 7.360 78 in units of $|e|$, at equilibrium between the quantum cluster and the embedding shell-model crystal. The nearest-neighbor Ba^{2+} ions come to equilibrium at positions (0.47, 0.47, 0.44), having relaxed from (0.5, 0.5, 0.5). This repre-

sents an oblate quadrupolar moment induced in the embedding crystal. This tendency of the crystal to screen the moment of the impurity is well known. The point-charge simulator q is positive, as if it were representing the $2p$ -like lobes of the electron hole. This is what is required to produce the energy-minimizing screening effect. The energy gain by relaxing nearest- (Ba^{2+}) and second- (F^-) neighbor ions, without quadrupole consistency, is 1.28 eV. Quadrupole consistency adds a further 0.55 eV. The final relaxation of second-neighbor F^- ions in the xy plane is (-0.07) , and of those on the z axis is (-0.13) . We therefore see that substitutional O^- induces a local contraction of the embedding host crystal. Here, all distances are in units of anion sublattice spacing. The contraction of the crystal about the impurity, noted above, may not be accurate, for two reasons. First, the KKLP for Ba^{2+} ions may not accurately represent the true interionic potentials in the quantum cluster. Second, interionic potentials within the quantum cluster may not be fully compatible with the Buckingham potentials by which the cluster is coupled to the embedding shell-model crystal.

We believe that it is instructive to see the effect on the F^- ion as it goes from free space into a perfect BaF_2 crystal. In Sec. II we described an iterative procedure for determining the optimized F^- basis set in BaF_2 . It turns out that the contraction coefficients $d_i(k)$, Eq. (8), in a (43/4) basis set¹¹ change only by about 1%. Nevertheless, the total cluster energy drops by about 2 eV.

We have estimated the basis set superposition error¹⁸ for the ground state of O^- in BaF_2 at the level where the basis set was minimal but optimized, and found it to be 0.9 eV, for a cluster of 69 electrons.

The effect on the ground-state energy of orbitals beyond the minimal set can be estimated from our work. Adding $3s$ orbitals to F^- and O^- , and $6s$ orbitals to Ba^{2+} , and optimizing them, reduces the Hartree-Fock energy by 2.4 eV, even though these orbitals have quite small occupancies as measured by Mulliken populations. The additional orbitals, namely, $3s$, $3p$, and $3d$ for F^- , $3s$, and $3d$ for O^- and $6s$ and $5d$ for Ba^{2+} , are not available from the literature,¹¹ even for free atoms. Our starting point in each case was to scale the radial part of a given orbital from that which is known for a filled-shell atom, using a scaling factor that is determined from an orbital type that is occupied in both species. For example, consider the $3d$ orbital for O^- . The nearest rare gas with an occupied $3d$ orbital is Kr. Both Kr and O have occupied $2s$ orbitals. The ratios of each of the three gaussian exponential coefficients, α , of their $2s$ contractions are evaluated, and these scaling factors are applied to the corresponding α 's of the Kr $3d$ orbital, keeping its $3d$ contraction coefficients fixed. In this way, we obtained plausible starting orbitals from which to carry out the optimization process. Similarly, having optimized orbitals in the ground state, their reoptimization in an excited state can have a large effect on the estimate of the excitation energy. For example, reoptimizing O^- - $3s$, Ba^{2+} - $6s$, and O^- - $3d$ orbitals in excited state (b) lowers the excitation by 0.08, 3.13, and 0.05 eV, respectively, for a total of 3.26 eV. Reoptimizing Ba^{2+} - $6s$ and O^- - $3d$ orbitals in excited state (c) lowers the excitation by 0.30 and 5.33 eV, respectively, for a total of 5.63 eV. Note then that such reoptimization also materially

TABLE II. Energies of O^- in BaF_2 (eV): ground state, excited states (b) and (c); Hartree-Fock level (E_{HF}); correlation correction, second-order MBPT (E_{CORR}); spin projection correction (E_s); total energies (E); transition energies (ΔE); absorption splitting (ΔE_{abs}). For E_{HF} , E , add ($-18\,200$ eV). Based on Ba^{2+} - $6s$ orbitals.

	E_{HF}	E_{CORR}	E_s	E	ΔE	ΔE_{abs}
Ground	-50.62	-14.15	0	-64.77		
(b)	-41.80	-14.18	0.16	-55.82	8.95	
(c)	-40.35	-15.02	0.35	-55.02	9.74	0.80

affects the estimate of absorption splitting. All these numbers are at the Hartree-Fock level.

Once an adequate basis set has been optimized in the ground state and in excited states (a), (b), and (c), as described in Sec. II, there remain two more steps to determine the optical excitation process. First we must evaluate the correlation correction, by second order MBPT in the present work. Then we must project excited states (b) and (c) orthogonal to state (a), in order to have results for spin- $\frac{1}{2}$ eigenstates. We reiterate that the full basis set used for the final results corresponds to F^- - $1s, 2s, 2p, 3s, 3p, 3d$; O^- - $1s, 2s, 2p, 3s, 3d$; Ba^{2+} - $6s$. A study was carried out using Ba^{2+} - $5d$ in place of $6s$. The optimized ground-state energy at Hartree-Fock level was 0.08 eV higher with $5d$ than with $6s$. Excited state levels (b) and (c) were 0.10 and 1.07 eV higher, respectively, but the qualitative nature of the transition was the same. We have therefore not carried the $5d$ -based calculations through correlation and spin projection stages. Complete results for the $6s$ -based calculations are given in Table II. We note that the correlation correction, ~ 15 eV, is substantial, reflecting the fact that the basis set is quite rich. We shall see shortly that this richness is essential to a correct understanding of the excitation process. While the correlation correction does not significantly affect the excitation in the spin-up manifold, case (b), it does affect case (c), and therefore the absorption splitting, substantially. The contribution of spin projection is smaller, but nevertheless significant.

It is worthwhile to extract data from Table II, to see the separate contributions to the excitation energies and to the absorption splitting from Hartree-Fock, correlation correction, and spin projection stages of the analysis. These results are given in Table III. We see that correlation reduces the absorption line splitting by more than half, and that spin projection works in the opposite direction, with a contribution of 0.2 eV. At this stage we recall that the fast luminescence of BaF_2 is at 195 and 220 nm,³ corresponding to 6.36 and 5.64 eV, respectively. Comparing with calculated absorption energies from Table III of 8.95 and 9.74 eV for O^-

TABLE III. Contributions (eV) to transition energies, $\Delta E(b)$ and $\Delta E(c)$, and to absorption splitting ΔE_{abs} , from Hartree-Fock (HF), correlation (CORR), and spin projection (s).

	HF	CORR	s	Total
$\Delta E(b)$	8.82	-0.04	0.16	8.95
$\Delta E(c)$	10.27	-0.88	0.35	9.74
ΔE_{abs}	1.44	-0.84	0.19	0.80

impurity, we conclude that the latter is not a candidate for explaining why the luminescent efficiency is degraded by radiation damage.

We can learn more about the O^- optical excitation process from the Fock eigenstates at the top of the occupied manifolds in ground and excited states (b) and (c). In the ground state, the top of both spin-up and spin-down occupied manifold are dominated by O^- $2p_{x,y}$ orbitals. Below them, the valence-band edge of the crystal is dominated by F^- $2p$ orbitals. In excited state (b) the last occupied spin-up orbital is predominately of F^- $3d$ character, while in state (c) the last occupied spin-down orbital is predominately of Ba^{2+} $6s$ character. The Mulliken populations, that give some indication of the number of electrons associated with each ion, support this picture. For case (b), the O^- , $(F^-)_6$ and $(Ba^{2+})_4$ Mulliken populations are 8.14, 60.62, and 0.24, respectively, i.e., approximately 8, 61, and zero, indicating an excitation in which about one electron is transferred from O^- (9 electrons) to the second-neighbor F^- ions. For case (c), the corresponding numbers are 8.31, 59.85, and 0.84, or approximately 8, 60, and 1, indicating an excitation from O^- to Ba^{2+} nearest neighbors. The strong deviation of the above Mulliken populations from integers indicates how limited it is to talk about this many-electron system in terms of single-electron states and processes. We note from the above analysis that there are no localized excited states of O^- in the band gap. On the other hand, the nature of the Fock eigenstates in the ground state, and the fact that the excitation, 8.95 and 9.74 eV, is significantly less than the band gap of BaF_2 of 10.48 eV, indicates that the O^- $2p_{x,y}$ level is localized above the valence band of the crystal.

The picture of the excitation that emerges from this analysis is quite interesting. Spin polarization associated with the prolate quadrupole moment of the substitutional O^- impurity locally deforms the conduction band of the BaF_2 crystal, exposing a F^- $3d$ -based state at the bottom of the spin-up part of the conduction band, and a Ba^{2+} $6s$ -based state at the bottom of the spin-down part, upon excitation. The two components of the split optical excitation of O^- represent corresponding transitions to the conduction band.

A possible alternative mechanism for optical absorption in the presence of oxygen impurity has been brought to our attention. It is an excitation from the valence band of the crystal to the unoccupied (spin down) $2p_z$ level of the O^- impurity. This may, in fact, be the lowest excitation. A rough assessment is based on the single-electron Fock eigenvalues, while acknowledging that these are quite inaccurate, quantitatively. For the ground state, the energy difference between the virtual Ba^{2+} $6s$ -like orbital and the occupied O^-

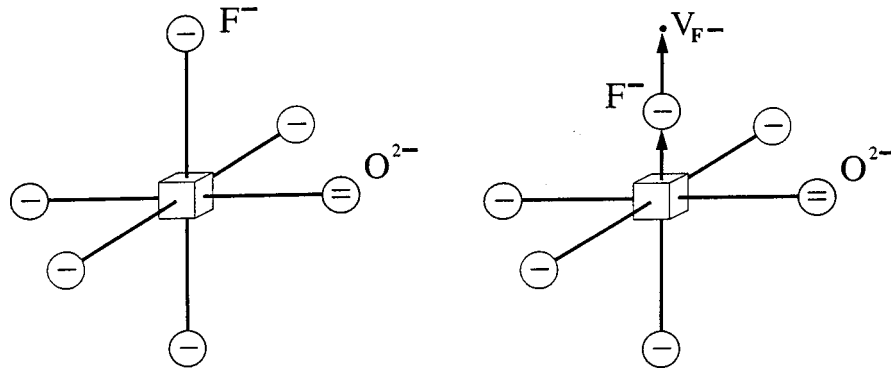


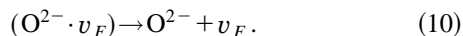
FIG. 2. Dissociation of $(\text{O}^{2-} \cdot v_F)$ oxygen-fluoride vacancy dipole defect complex in BaF_2 crystal. Initial configuration on the left, activated configuration on the right.

$2p_{x,y}$ -like orbital is ~ 25 eV, while the difference between the virtual $\text{O}^- 2p_z$ -like orbital and the highest even-parity valence orbital, $\text{F}^- 2p$ -like, is ~ 21 eV. The former figure, 25 eV, translates into a many-body excitation energy of 9.7 eV, indicating the hazard of using Fock eigenvalues. On the other hand, the difference between 25 and 21 eV supports the idea that the valence band-to-impurity excitation deserves analysis, in addition to F -center excitation, in studying radiation damage effects in this material.

It is worthwhile to summarize at this point some of the things that we have learned about the method as we have built up accuracy of the physical model and the computational approach. For each of the following features, qualitative results obtained from the rougher levels of approximation differ from those of the more accurate final calculations. (1) The ion-size effect of Ba^{2+} , contrasting point-ion with KKLP pseudopotentials. (2) The quadrupole moments induced first in the O^- ion, and second through total-energy minimization into the embedding crystal, by spin polarization. (3) The use of an adequate nonminimal basis set, optimized with respect to contraction and exponential components, while being constrained from excessive diffuseness. (4) Correlation (second-order MBPT). (5) Projection of excited states orthogonal to the low-lying forbidden spin eigenstate. Careful treatment of all of the above features together represents a new standard in our own simulation work, and we suspect with respect to the work of other authors also. We have demonstrated that without this level of care, not only is quantitative prediction unreliable, but so even is qualitative understanding.

IV. O^- PRODUCTION BY RADIATION DAMAGE

In Sec. I we described the radiation damage process whereby a $(\text{O}^{2-} \cdot v_F)$ defect complex is dissociated upon absorption of energy $h\nu$, and the dissociated components are stabilized in the crystal by electron transfer from O^{2-} to v_F leaving free O^- ions and F centers, F_c . In this section we report two calculations relating to this process. First, we calculate the activation energy for dissociation:



Second, we compare the final state total energy of Eq. (10) when O^{2-} and v_F are well separated, with the total energy of well-separated O^- and F_c , after electron transfer has oc-

curred. Throughout this section, the standard of treatment, both in terms of basis sets and of cluster atom positions, is not comparable with that of Sec. III. Correspondingly, only qualitative, or roughly quantitative results are presented.

In Fig. 2, we show the activated and initial configurations for $(\text{O}^{2-} \cdot v_F)$ dissociation, in which the vacancy moves from a nearest to a second-neighbor site on the fluoride sublattice. In each configuration, the ions shown, and four Ba^{2+} ions, constitute the quantum cluster. As in Sec. III, this cluster is embedded in an infinite shell-model BaF_2 crystal whose deformation and polarization are consistent with the cluster. Some details of this calculation are in order. First the basis set, unlike that developed in Sec. III, is minimal except for the addition of $\text{F}^- 3s$ and $\text{Ba}^{2+} 6s$ orbitals. The O^{2-} and F^- orbitals used here were free neutral oxygen and free F^- ($4\ 3/4$) orbitals taken from Ref. 11. Furthermore, $\text{F}^- 2p$ orbitals are decontracted from one contraction of four primitive atomic orbitals, to two of two each, increasing their polarizability. For the initial configuration, we need to include displacement of O^{2-} from the perfect-crystal F^- site, and dipole consistency between the $(\text{O}^{2-} \cdot v_F)$ complex and the embedding crystal. We have felt that these effects would be more accurately represented in a cluster that is centered on the O^{2-} ion, with one F^- site vacant, so that the O^{2-} sees all four of its nearest-neighbor Ba^{2+} ions and its five second-neighbor F^- ions. Accordingly, results from such a calculation were transferred to the initial-state calculation for Fig. 2. In calculations for Fig. 2, O^{2-} - Ba^{2+} and O^{2-} - F^- Buckingham potentials are needed. For this we have used the O^- - Ba^{2+} potential described in Sec. II, and the F^- - F^- potential, respectively. For the activated configuration, the diffusing F^- ion was placed halfway between lattice sites. In this configuration, the dipole moment of the defect is not dominant, and therefore dipole consistency in terms of point charge simulators was not maintained. Rather, the point charge simulators for ions of the cluster determined consistency with the embedding crystal's polarization. In both initial and activated configurations, a $1s$ vacancy-centered orbital was included, taken from the isolated F -center calculation in which it was optimized. In the initial state, F^- and Ba^{2+} ion positions were taken at perfect crystal sites. In the activated configuration, the two Ba^{2+} ions were relaxed in the direction radially from the diffusing F^- ion, and the O^{2-} ion's displacement on the original defect dipole axis was reoptimized. The corresponding lowerings of total en-

TABLE IV. Calculated Hartree-Fock total energies (eV) of point defects at F^- sites in BaF_2 : O^- , F center (F_c), O^{2-} , fluoride vacancy (v_F). All energies have been increased by 18 200 eV.

Defect	Total energy	Sums
O^-	-46.28	
F_c	-12.11	-58.39
O^{2-}	-45.11	
v_F	-11.86	-56.96

ergy were 0.08 and 0.48 eV, respectively. We have gone into this detail so that the reader will know that, although the calculations are somewhat rudimentary, nevertheless most of the significant physical effects have been included with some accuracy.

The calculated activation energy for $(O^{2-} \cdot v_F)$ dissociation, Fig. 2, is 0.93 eV at the Hartree-Fock level. First, not surprisingly, this is positive; that is, the bound complex of the initial state, Fig. 2, is stable, compared to dispersed O^{2-} and v_F point defects. Second, the calculated value is reasonable, comparable with vacancy activation energies in typical oxides and halides: a confirmation of the qualitative validity of the rudimentary method used. We note that this is our first calculation of an activation energy for ionic diffusion based entirely on an embedded quantum cluster, rather than on the more usual use of the shell model, whose impurity parameters may be based on subsidiary quantum cluster calculations.²⁰ (Our analysis of the quantum diffusion of muonium^{21,22} is not comparable, where not only the electrons but also the μ^+ nucleus are treated quantum-mechanically.)

We now consider the stability of highly dilute O^- ions and F centers (F_c), compared to highly dilute O^{2-} ions and fluoride vacancies (v_F), see Eq. (2). For this, we do four calculations, with the cluster of Fig. 1, in which O^- is successively replaced by F_c , O^{2-} , and v_F . In all these calculations, the basis set that was used for the $(O^{2-} \cdot v_F)$ complex above is augmented with F^- $3s$ orbitals, and the F^- and Ba^{2+} ion positions are relaxed to equilibrium. The F -center basis, consisting of a single $1s$ orbital, was optimized. In the present work our analysis of the F center is clearly incomplete and so we have not calculated any of its properties such as, for example, isotropic hyperfine constants. The results at Hartree-Fock level are given in Table IV. We see that the stabilization energy is calculated to be 1.4 eV. This supports the idea that radiation damage dissociates $(O^{2-} \cdot v_F)$ defect complexes, ultimately producing free O^- ions, Sec. III, and F centers.

The electronic distributions for some of these point defects, as indicated by Mulliken populations, are interesting. For the F -center cluster, they are as follows: F_c 0.9476, 4 Ba^{2+} 0.2208, 6 F^- 59.8320. Thus there is slight charge transfer from F_c and F^- to Ba^{2+} around the defect. For v_F : v_F 0.0288, 4 Ba^{2+} 0.0784, 6 F^- 59.8926. Thus there is slight charge transfer from F^- to v_F and Ba^{2+} around the defect. These results are reasonable, given what we know about F centers and vacancies in other ionic crystals. Finally, we have for O^{2-} : O^{2-} 9.3857, 4 Ba^{2+} 0.3856, 6 F^- 60.2286. We conclude that O^{2-} in BaF_2 has a good fraction of one electron distributed on its first and second neighbors. This is in agreement with our determination that dilute O^{2-} and v_F

are an unstable combination, as in Eq. (2): O^{2-} has a strong tendency to lose one electron to the (mostly Ba^{2+} part of the) conduction band. Finally, we note the Mulliken populations of the defect complex $(O^{2-} \cdot v_F)$ in the stable configuration, Fig. 2. They are as follows: v_F 0.1567, O^{2-} 9.4560, 4 Ba^{2+} 0.3400, 5 F^- 50.0472. Again we see the spreading of a good fraction of one electron onto the neighbors of the oxygen ion, nominally $(2-)$, and into the adjacent vacancy.

V. SUMMARY

We have studied the radiation damage process in BaF_2 in relation to oxygen impurity and loss of luminescent transmissivity. The optical absorption of the free O^- ion, at 8.95 and 9.74 eV, has been found to occur from a localized oxygen $2p$ -like state in the band gap to the conduction manifold of the host crystal. This manifold is locally spin polarized, so that the transitions involve fluoride $3d$ -like and barium $6s$ -like parts of the conduction band, respectively. Since these absorption energies are about 3 eV (50%) above the fast luminescence of BaF_2 crystal, one concludes that O^- is not involved in the degradation of luminescent transmissivity.

Our calculations show that oxygen in BaF_2 is stable in an $(O^{2-} \cdot v_F)$ defect complex whose activation energy for dissociation is ~ 1 eV: calculated at 0.93 eV. However, a dilute combination of free O^{2-} ions and fluoride vacancies is unstable against the electron transfer process that results in O^- ions and F centers, the energy difference being calculated at 1.4 eV per oxygen ion. From the above results we conclude that, to the extent that oxygen is involved, it must be F centers that absorb the intrinsic luminescence of BaF , following radiation damage. While these conclusions have been noted in the literature for some time, this work provides the first quantitative verification. If it were of sufficient importance, one could carry out an analysis of the optical excitation of the F center, along the lines used here for O^- , Secs. II and III.

We believe that this work contributes significantly to the methodology of simulating the optical properties of impurities in insulating crystals, by demonstrating the importance of the ion-size effect for heavy cations, of basis set optimization in all electronic states, and of correlation correction and spin projection. Other essential features of the simulation are spin polarization of the electronic distribution, and distortion and polarization of the host crystal. Analyses that fail to include the above features accurately and with mutual consistency may well arrive at conclusions that are not merely quantitatively incorrect, but also qualitatively incorrect.

ACKNOWLEDGMENTS

The authors thank M. Bromirski for assistance with some calculations. We acknowledge financial support as follows: J.M.V.-NSERC of Canada, Winnipeg Institute of Theoretical Physics, and Manitoba Education and Training; T.L.-Faculty of Science, University of Manitoba; M.G.-Department of Physics at Michigan Technological University, and National Natural Science Foundation of China Grant No. 19117531.

- ¹*Scintillator and Phosphor Materials*, edited by M. J. Weber, P. Lecoq, R. C. Ruchti, C. Woody, W. M. Yen, and R. Y. Zhu, MRS Symposia Proceedings No. 348 (Materials Research Society, Pittsburgh, 1994).
- ²K. H. Xiang, R. Pandey, and J. M. Vail (unpublished).
- ³R. Y. Zhu, Nucl. Instrum. Methods Phys. Res. A **340**, 442 (1994).
- ⁴For example, L. K. Ermakov, P. A. Rodnyi, and N. V. Starostin, Fiz. Tverd. Tela **33**, 2542 (1991) [Sov. Phys. Solid State **33**, 1435 (1991)].
- ⁵For example, D. A. Ma, R. Y. Zhu, and H. Newman, Nucl. Instrum. Methods Phys. Res. A **356**, 309 (1995).
- ⁶S. Ron, G. Chen, F. Zhang, and Y. Zheng, in *Scintillator and Phosphor Materials* (Ref. 1), p. 435.
- ⁷L. M. Wang, L. Y. Chen, and X. Wu, in *Scintillator and Phosphor Materials* (Ref. 1), p. 399.
- ⁸L. Y. Chen, M. Gu, L. M. Wang, and K. H. Xiang, in *Scintillator and Phosphor Materials* (Ref. 1), p. 447.
- ⁹E. Radzhabov and P. Figura, Phys. Status Solidi B **186**, K37 (1994).
- ¹⁰J. Andriessen, P. Dorenbos, and C. W. E. van Eijk, Mol. Phys. **74**, 535 (1991).
- ¹¹S. Huzinaga, *Handbook of Gaussian Basis Sets* (Elsevier, New York, 1985).
- ¹²C. R. A. Catlow, M. J. Norgett, and A. Ross, J. Phys. C **10**, 1627 (1977).
- ¹³J. H. Harker, A. H. Harding, P. B. Keegstra, R. Pandey, J. M. Vail, and C. Woodward, Physica B **131**, 151 (1985).
- ¹⁴J. M. Vail, R. Pandey, and A. B. Kunz, Rev. Solid State Sci. **5**, 241 (1991).
- ¹⁵D. J. Thouless, *The Quantum Mechanics of Many-Body Systems*, 2nd ed. (Academic, New York, 1972), Ch. IV, Sec. 1.
- ¹⁶J. M. Vail, J. Phys. Chem. Solids **51**, 589 (1990).
- ¹⁷A. B. Kunz and D. L. Klein, Phys. Rev. B **17**, 4614 (1978).
- ¹⁸See, for example, A. Szabo and N. S. Ostlund, *Modern Quantum Chemistry* (McGraw-Hill, New York, 1989).
- ¹⁹L. Seijo and Z. Barandiaran, Int. J. Quantum Chem. **60**, 617 (1996).
- ²⁰J. Meng, R. Pandey, J. M. Vail, and A. B. Kunz, J. Phys.: Condens. Matter **1**, 6049 (1989).
- ²¹J. M. Vail, T. McMullen, and J. Meng, Phys. Rev. B **49**, 193 (1994).
- ²²T. McMullen, J. Meng, J. M. Vail, and P. Jena, Phys. Rev. B **51**, 15 879 (1995).